Laser link acquisition demonstration for the GRACE Follow-On mission

Danielle M. R. Wuchenich,[1,*] Christoph Mahrdt,[2] Benjamin S. Sheard,[2] Samuel P. Francis,[1] Robert E. Spero,[3] John Miller,[1] Conor M. Mow-Lowry,[1] Robert L. Ward,[1] William M. Klipstein,[3] Gerhard Heinzel,[2] Karsten Danzmann,[2] David E. McClelland,[1] and Daniel A. Shaddock[1]

[1] *Centre for Gravitational Physics, Department of Quantum Science, The Australian National University, Canberra, ACT 0200, Australia*
[2] *Max Planck Institute for Gravitational Physics (Albert Einstein Institute) and Institute for Gravitational Physics, Leibniz Universität Hannover, Callinstraße 38, 30167, Germany*
[3] *Jet Propulsion Laboratory, California Institute of Technology, 4800 Oak Grove Drive, Pasadena, CA, 91109, USA*
[*] *danielle.wuchenich@anu.edu.au*

Abstract: We experimentally demonstrate an inter-satellite laser link acquisition scheme for GRACE Follow-On. In this strategy, dedicated acquisition sensors are not required—instead we use the photodetectors and signal processing hardware already required for science operation. To establish the laser link, a search over five degrees of freedom must be conducted ($\pm$ 3 mrad in pitch/yaw for each laser beam, and $\pm$ 1 GHz for the frequency difference between the two lasers). This search is combined with a FFT-based peak detection algorithm run on each satellite to find the heterodyne beat note resulting when the two beams are interfered. We experimentally demonstrate the two stages of our acquisition strategy: a $\pm$ 3 mrad commissioning scan and a $\pm$ 300 μrad reacquisition scan. The commissioning scan enables each beam to be pointed at the other satellite to within 142 μrad of its best alignment point with a frequency difference between lasers of less than 20 MHz. Scanning over the 4 alignment degrees of freedom in our commissioning scan takes 214 seconds, and when combined with sweeping the laser frequency difference at a rate of 88 kHz/s, the entire commissioning sequence completes within 6.3 hours. The reacquisition sequence takes 7 seconds to complete, and optimizes the alignment between beams to allow a smooth transition to differential wavefront sensing-based auto-alignment.

OCIS codes: (120.3180) Interferometry; (120.6085) Space instrumentation; (120.1880) Detection; (120.3930) Metrological instrumentation.

References and links

1. B. Tapley, S. Bettadpur, M. Watkins, and C. Reigber, "The gravity recovery and climate experiment: Mission overview and early results," Geophys. Res. Lett **31,** L09607 (2004).
2. B. D. Tapley, S. Bettadpur, J. C. Ries, P. F. Thompson, and M. M. Watkins, "GRACE Measurements of Mass Variability in the Earth System," Science **305**, 503–505 (2004).
3. J. Wahr, S. Swenson, V. Zlotnicki, and I. Velicogna, "Time-variable gravity from GRACE: First results," Geophys. Res. Lett. **31,** L11501 (2004).

#208685 - $15.00 USD Received 25 Mar 2014; accepted 22 Apr 2014; published 2 May 2014

4. A. Lombard, D. Garcia, G. Ramillien, A. Cazenave, R. Biancale, J. Lemoine, F. Flechtner, R. Schmidt, and M. Ishii, "Estimation of steric sea level variations from combined GRACE and Jason-1 data," Earth and Planetary Science Letters **254**, 194–202 (2007).
5. M. Rodell, I. Velicogna, and J. Famiglietti, "Satellite-based estimates of groundwater depletion in India," Nature **460,** 999–1003 (2009).
6. S. Luthcke, H. Zwally, W. Abdalati, D. Rowlands, R. Ray, R. Nerem, F. Lemoine, J. McCarthy, and D. Chinn, "Recent Greenland ice mass loss by drainage system from satellite gravity observations," Science **314**, 1286–1289 (2006).
7. G. Ramillien, A. Lombard, A. Cazenave, E. R. Ivins, M. Llubes, F. Remya, and R. Biancale, "Interannual variations of the mass balance of the Antarctica and Greenland ice sheets from GRACE," Global Planet. Change **53**, 198–208 (2006).
8. I. Velicogna, "Increasing rates of ice mass loss from the Greenland and Antarctic ice sheets revealed by GRACE," Geophys. Res. Lett **36,** L19503 (2009).
9. T. Jacob, J. Wahr, W. Pfeffer, and S. Swenson, "Recent contributions of glaciers and ice caps to sea level rise," Nature **482,** 514–518 (2012).
10. B. Sheard, G. Heinzel, K. Danzmann, D. Shaddock, W. Klipstein, and W. Folkner, "Intersatellite laser ranging instrument for the GRACE follow-on mission," Journal of Geodesy **86**, 1083–1095 (2012).
11. The GRACE-C Interferometer team, "The GRACE-C interferometer," technical note, the Albert Einstein Institute (2011).
12. NASA Earth Science Decadal Survey Studies, "GRACE II : Gravity Recovery and Climate Experiment," (2009), http://decadal.gsfc.nasa.gov/grace2.html.
13. The LISA Project, "LISA Pre-Phase A Report," technical note, the Albert Einstein Institute (1998).
14. G. M. Harry, P. Fritschel, D. A. Shaddock, W. Folkner, and E. S. Phinney, "Laser interferometry for the Big Bang Observer," Classical and Quantum Gravity **23,** 4887–4894 (2006).
15. R. Lange and B. Smutny, "Optical inter-satellite links based on homodyne BPSK modulation: heritage, status, and outlook," in *Free-Space Laser Communication Technologies XVII*, G. Stephen Mecherle, ed., Proc. SPIE **5712**, 1–12 (2005).
16. B. Smutny, R. Lange, H. Kämpfner, D. Dallmann, G. Mühlnikel, M. Reinhardt, K. Saucke, U. Sterr ; B. Wandernoth, R. Czichy, "In-orbit verification of optical inter-satellite communication links based on homodyne BPSK," in *Free-Space Laser Communication Technologies XX*, Stephen Mecherle, ed., Proc. SPIE **6877,** 687702 (2008).
17. F. Heine, H. Kämpfner, R. Czichy, R. Meyer, and M. Lutzer, "Optical inter-satellite communication operational," in *Military Communications Conference MILCOM 2010,* San Jose, California, USA, pp. 1583–1587 (2010).
18. M. Gregory, F. Heine, H. KŁmpfner, R. Meyer, R. Fields, C. Lunde, "Tesat Laser Communication Terminal Performance results on 5.6 Gbit Coherent Inter Satellite and Satellite to Ground Links," in *International Conference on Space Optics 2010*, Rhodes Island, Greece, 4-8 Oct. 2010.
19. C. Mahrdt, "Status Laser Link Acquisition at AEI," presented at the *GRACE Follow-On Workshop,* Heron Island, Australia, Sept. 2012.
20. C. Mahrdt, *Laser Link Acquisition for the GRACE Follow-On Laser Ranging Interferometer,* Ph.D. thesis, Albert Einstein Institute (2013).
21. F. Ales, P. Gath, U. Johann, and C. Braxmaier, "Modeling and Simulation of a Laser Ranging Interferometer Acquisition and Guidance Algorithm," in *American Institute of Aeronautics and Astronautics GNC Conference,* Boston, USA, 2013.
22. F. Ales, P. Gath, U. Johann, and C. Braxmaier, "Modeling and Simulation of a Laser Ranging Interferometer Acquisition and Guidance Algorithm," Journal of Spacecraft and Rockets **51,** 226–238 (2014).
23. F. Cirillo and P. F. Gath, "Control system design for the constellation acquisition phase of the LISA mission," J. Phys.: Conf. Ser. **154,** 012014 (2009).
24. W. M. Folkner, G. de Vine, W. M. Klipstein, K. McKenzie, D. Shaddock, R. Spero, R. Thompson, D. Wuchenich, N. Yu, M. Stephens, J. Leitch, M. Davis, J. de Cino, C. Pace, and R. Pierce, "Laser Frequency Stabilization for GRACE-II," in *Proceedings of the 2010 Earth Science Technology Forum* (2010).
25. W. M. Folkner, G. de Vine, W. M. Klipstein, K. McKenzie, R. Spero, R. Thompson, N. Yu, M. Stephens, J. Leitch, R. Pierce, T. T.-Y. Lam, and D. Shaddock, "Laser frequency stabilization for GRACE-2," in *Proceedings of the 2011 Earth Science Technology Forum* (2011).
26. R. Pierce, J. Leitch, M. Stephens, P. Bender, and R. Nerem, "Intersatellite range monitoring using optical interferometry," Appl. Opt. **47**, 5007–5019 (2008).
27. D. Shaddock, B. Ware, P. G. Halverson, R. E. Spero, and B. Klipstein, "Overview of the LISA Phasemeter," AIP Conference Proceedings **873**, 654–660 (2006).
28. E. Morrison, B. J. Meers, D. I. Robertson, and H. Ward, "Automatic alignment of optical interferometers," Appl. Opt. **33**, 5041–5049 (1994).
29. P. Fritschel, N. Mavalvala, D. Shoemaker, D. Sigg, M. Zucker, and G. González, "Alignment of an Interferometric Gravitational Wave Detector," Appl. Opt. **37**, 6734–6747 (1998).
30. G. Heinzel, V. Wand, A. García, O. Jennrich, C. Braxmaier, D. Robertson, K. Middleton, D. Hoyland, A. Rüdiger, R. Schilling, U. Johann, and K. Danzmann, "The LTP interferometer and phasemeter," Classical and Quantum

#208685 - $15.00 USD Received 25 Mar 2014; accepted 22 Apr 2014; published 2 May 2014

Gravity **21**, S581 (2004).
31. G. Heinzel, C. Braxmaier, M. Caldwell, K. Danzmann, F. Draaisma, A. García, J. Hough, O. Jennrich, U. Johann, C. Killow, K. Middleton, M. te Plate, D. Robertson, A. Rüdiger, R. Schilling, F. Steier, V. Wand, and H. Ward, "Successful testing of the LISA Technology Package (LTP) interferometer engineering model," Classical and Quantum Gravity **22**, S149 (2005).
32. H. Langenbach and M. Schmid, "Fast steering mirror for laser communication," in *11th European Space Mechanisms and Tribology Symposium, ESMATS 2005,* B. Warmbein, ed., Vol. 591 of ESA Special Publication, pp. 27–33 (2005).
33. D. Wuchenich, *Inter-satellite laser interferometry,* Ph.D. thesis, The Australian National University (2014).
34. Kirk McKenzie, Jet Propulsion Laboratory, California Institute of Technology, 4800 Oak Grove Drive, Pasadena, CA, 91109 (personal communication, 2013).
35. J. Chitode, *Principles Of Communication* (Technical Publications, Pune, 2009).

1. Introduction

The Gravity Recovery and Climate Experiment (GRACE) satellites have been monitoring key aspects of our climate since their launch in 2002 [1, 2]. These twin satellites fly 200 km apart in a polar, low-Earth orbit and employ a microwave instrument to continuously track changes in their separation with micron-level sensitivity. These displacement measurements (along with GPS and accelerometer data) have been used to produce monthly models of Earth's gravity field [3]. Geoscientists have used this data to track water movement, such as changes in sea levels [4] and continental ground water [5], and over the past decade have quantified climate change phenomena, such as the melting of polar ice [6–9].

A new mission, GRACE Follow-On (GFO), is planned to include a laser ranging instrument based on a laser interferometer as a technology demonstrator to improve the inter-satellite displacement measurement by up to a factor of 25 [10, 11]. Laser interferometry is the preferred candidate for satellite ranging and will likely be utilized in future space missions, such as for gravity observations/geodesy missions (e.g. GRACE Follow-On [10], GRACE-II [12]) and space-based gravitational wave detectors (LISA [13], BBO [14]).

On GRACE Follow-On, the satellites will exchange laser beams and will use heterodyne interferometry to infer the change in their separation in the same way that the microwave instrument does on the original GRACE mission. Before science operation can begin, the laser on each satellite needs to be precisely pointed (in both pitch & yaw) towards the opposite satellite, and the laser frequencies must differ by less than the photodetector bandwidth (a frequency difference of 1 part in 10^7, or ~ 20 MHz). The acquisition strategy to establish this link must therefore scan each of the 5 degrees of freedom over its respective uncertainty range.

Acquisition is a challenging problem and extensive simulations have been performed for generic inter-satellite laser links (e.g. laser communication terminals on TerraSAR-X or NFIRE) [15–18], as well as specifically for GRACE Follow-On [19–22] and the proposed gravitational wave detector LISA [23]. The GFO strategy differs from these other acquisition schemes as it cannot utilize dedicated hardware or acquisition sensors, but instead must rely on the photodetector and signal processing hardware already required for science operation.

The GFO acquisition strategy implemented in our experiment combines spatial/frequency scanning with a fast Fourier transform (FFT)-based peak detection algorithm run on each satellite to find the alignment points and laser crystal temperature which produced the highest beat note amplitude (resulting from the interference between the two beams). This approach was developed based on high fidelity simulations conducted over several years led by Mahrdt at the Albert Einstein Institute [19, 20] in collaboration with the Australian National University and the Jet Propulsion Laboratory (JPL). Our acquisition approach is broken into two parts: a commissioning scan and a reacquisition scan. The commissioning scan is a large-range scan envisaged to be performed once after launch, and will take significantly longer and may require input from the ground. The reacquisition scan is a smaller-range, faster scan that will be used

#208685 - $15.00 USD Received 25 Mar 2014; accepted 22 Apr 2014; published 2 May 2014

after the initial uncertainties are reduced by the commissioning scan, and is designed to be autonomous.

In this paper, we experimentally demonstrate an acquisition system with GRACE Follow-On-like parameters. This point design and our experimental results were presented as the candidate acquisition architecture at NASA's Preliminary Design Review for the GRACE Follow-On laser ranging instrument at JPL in May 2013.

2. The GRACE Follow-On laser ranging instrument

A detailed conceptual design of the GFO laser ranging instrument, along with the instrument description, is provided in [10]. Here we briefly summarize some of the components on each satellite relevant to acquisition:

- **Laser** with ≈ 1 μm wavelength, which can be frequency stabilized to the on-board reference cavity.
- **Fast steering mirror (FSM)** to control the laser beam pointing in pitch and yaw to continuously track the other satellite by optimizing the interferometric contrast, while compensating for any attitude jitter and orbit perturbations.
- **Beam splitter** to interfere the local beam with laser light received from the distant satellite.
- **Quadrant photodetector (QPD)** to detect the interference between the two beams at the heterodyne frequency.
- **Phasemeter** to measure the phase of the heterodyne beat note on each satellite produced from the interference between the local and distant beams. The phase of the beat note provides information about the spacecraft separation and the laser beam alignment. The phasemeter is implemented on a field programmable gate array (FPGA), which is also used for the acquisition.

The laser's frequency on one of the satellites will be stabilized to its on-board reference cavity [24,25]; we will refer to this as the master laser. The interferometer will be operated in an active transponder configuration, where the slave laser (the laser on the other satellite) will ultimately be offset phase-locked to the incoming light from the master laser [26]. Conceptually, the distant satellite acts like an amplifying mirror, where the phase of the received light is preserved and the signal is amplified and returned to the local satellite. The offset frequency is selected to reduce technical noise in the phase-locking and keep the beat note between $2-18$ MHz (the bandwidth of the electronics). This frequency varies due to the Doppler shift as the satellites' relative velocities vary in their orbit. As each satellite will have a reference cavity, the master/slave roles can be switched if, for example, one of the reference cavities fails.

Imaging optics will focus the interfered beams onto the QPD while mapping any tilt in both the local beam and in the received beam from the distant satellite to tilt at plane of the detector. Each satellite will record the phase of the heterodyne beat note via a digitally-implemented phasemeter [27]. The inter-satellite displacement measurement—the desired science measurement—can be recovered from the average phase measurements on each detector. Note that there will be one phasemeter channel per quadrant. The phases of the quadrants contain alignment information between the local and distant beams, allowing the steering mirror pointing to be corrected in closed-loop to keep the interferometers optimally aligned. This approach—differential wavefront sensing—is based on a standard alignment technique [28] developed for ground-based gravitational wave detectors [29] and is used in systems such as LISA Pathfinder [30,31].

#208685 - $15.00 USD Received 25 Mar 2014; accepted 22 Apr 2014; published 2 May 2014

3. Commissioning & reacquisition scans

After the GFO satellites are first launched, there will be an initial unknown offset between the interferometer axis and the on-board pointing estimate provided by the Attitude and Orbit Control System. This offset is estimated to be up to ± 3 mrad on each satellite. Recall that in addition to this beam pointing uncertainty, there will be an unknown offset between the laser's frequency on each satellite, estimated to be up to $f_{unc} = \pm 1$ GHz, much larger than the bandwidth of the detector electronics. Thus a commissioning scan is required to initially establish the laser link while scanning over these 5 degrees of freedom.

The goal of the acquisition is to bring the frequency offset between the lasers to within ~ 20 MHz while aligning the two beams well enough such that the transition to differential wavefront sensing on each satellite can be established. One objective is to minimize the time needed for the commissioning scan, making the speed at which the steering mirror can move between points a key determining factor for the total commissioning time. Effects which motivate a short commissioning time—such as orbit prediction errors—are examined in Mahrdt's analysis [20].

During the commissioning scan, both satellites will perform spatial scans by changing the pointing of their steering mirrors to scan the laser beam axis over a $R_{uc} = 3$ mrad uncertainty cone radius. Figure 1 shows a schematic of the signal processing hardware as well as a block diagram of the acquisition algorithm implemented on the phasemeter FPGA used in either the commissioning or reacquisition scans.

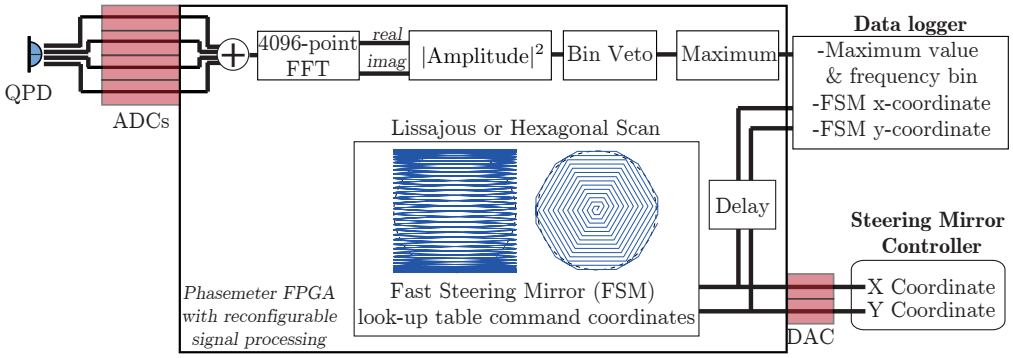

Fig. 1. Signal processing for the commissioning and reacquisition scans implemented in our experiment. Operations in the large rectangular box performed on an FPGA. The electronic delay in the FSM command coordinates path (going to the data logger) is to account for the computation time of the FFT. **QPD:** quadrant photodetector, **ADC:** analog-to-digital converter, **FPGA:** field programmable gate array, **FFT:** fast Fourier transform, **DAC:** digital-to-analog converter.

Simulations [20] predict that we can tolerate a maximum simultaneous misalignment of each steering mirror of up to $r_{wc} = 142$ µrad and still meet the minimum carrier-to-noise-density requirement per quadrant to ensure phasemeter tracking. Thus all possible spatial scan point combinations between the satellites will be covered with $r_{wc} = 142$ µrad resolution. Each quadrant is digitized by an analog-to-digital converter (ADC) and sent to the on-board FPGA for peak detection. In science operation, each quadrant will have its own channel for phasemeter processing. In acquisition mode, however, each quadrant will be digitized and then added with the signals from the other quadrants to form a sum on the FPGA mimicking a single element detector. A 4096-point FFT is continuously performed on this summed channel on each satellite during the scanning. After each FFT, the bin with the highest amplitude is recorded, along

#208685 - $15.00 USD Received 25 Mar 2014; accepted 22 Apr 2014; published 2 May 2014

with the corresponding steering mirror angle.

Certain frequency bins in the FFT may be vetoed before the peak detection algorithm chooses the bin with the highest value. If certain bins have more noise on GFO, due to electronic spurs or laser intensity noise for example, the statistics of the peak detection algorithm will be biased and these noisy bins will be chosen more frequently, even when no beat note is present. Depending on the intensity noise characteristics of the flight lasers, the level of the noise in these low frequency bins could even be higher than the beat note signals found during acquisition. Thus a bin veto will be performed on the FPGA after every FFT before the maximum value is picked, denoted as the *Bin Veto* stage in Fig. 1.

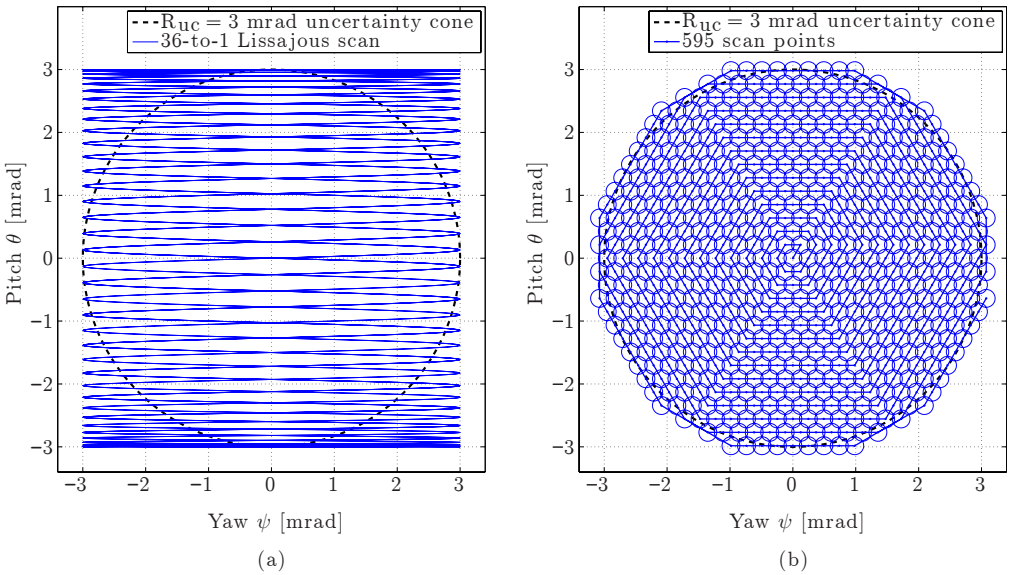

Fig. 2. Steering mirror scan patterns covering $R_{uc} = 3$ mrad with $r_{wc} = 142$ µrad resolution. (a) 36-to-1 Lissajous scan on steering mirror FSM1; (b) 595 point hexagonal scan on steering mirror FSM2. The hexagonal steering mirror will dwell at each point in its scan long enough to allow the Lissajous steering mirror to cover an entire R_{uc} scan. During the spatial scanning, the frequency of the slave laser will be slowly swept, and the spatial scanning sequence will repeat until the entire frequency uncertainty range f_{unc} has been covered.

As the total acquisition time in this approach is limited by the steering mirror scanning speed, optimizing the scan patterns to cover all scanning point combinations as quickly as possible becomes critical. One steering mirror will be driven with a fast Lissajous figure, while the other steering mirror will cover the uncertainty cone with a slower hexagonal scan pattern, as shown in Fig. 2. The Lissajous scan will have the fast-to-slow axis frequency ratio of $f_{fast\,axis}/f_{slow\,axis} = 36$ to give the r_{wc} resolution. The steering mirror with the hexagonal scan will dwell at each of the points in its scan long enough to allow the Lissajous steering mirror to cover its entire R_{uc} uncertainty space. During this spatial scanning, the frequency of the slave laser will be slowly swept. The slave laser's frequency should be swept at a rate such that the beat note frequency does not move by more than the bandwidth of the electronics per complete spatial scan. After all spatial scanning point combinations have been covered, the spatial scanning sequence will repeat until the entire frequency uncertainty range f_{unc} has been covered.

The data saved from the commissioning scan—the maximum bin and amplitude from each FFT, along with the corresponding steering mirror angles and slave laser temperature—will likely be downlinked to Earth for analysis to find the combination that produced the highest

#208685 - $15.00 USD Received 25 Mar 2014; accepted 22 Apr 2014; published 2 May 2014

beat note amplitude. From this we can estimate the offsets between the star tracker frame and the interferometer axis as well as the nominal laser frequency differences. Once these values are found, commands will be uplinked to the steering mirror angles and slave laser frequency control that will align the steering mirrors to better than 300 μrad in the four spatial degrees of freedom, as well as align the laser frequencies to close to 20 MHz. Note that the strategy was designed to be completed without communication between satellites or the ground, with the option to transition directly to science operation autonomously. If analyzed on the ground, however, the offsets settings will be uplinked sometime after the commissioning scan, perhaps the next day.

To further optimize the alignments, after the commissioning scan coordinates have been uplinked a *reacquisition* scan will be conducted—a smaller, faster spatial and frequency scan—to confirm the commissioning results and optimize the signal-to-noise ratio. After this reacquisition sequence is completed, the steering mirror will be steered to the position corresponding to the maximum detector output and wavefront sensing-based alignment will be initiated allowing science operation to commence. This reacquisition scan can potentially be utilized automatically every time the interferometer loses lock without intervention from the ground.

4. Experimental demonstration

We have designed and built an experiment to demonstrate the acquisition strategy described in the previous section and verify key simulation results. A simplified schematic of the experiment is shown in Fig. 3. The complete experimental layout and characterization is described in [33]. The experiment was designed to capture the relevant characteristics of the GFO laser ranging

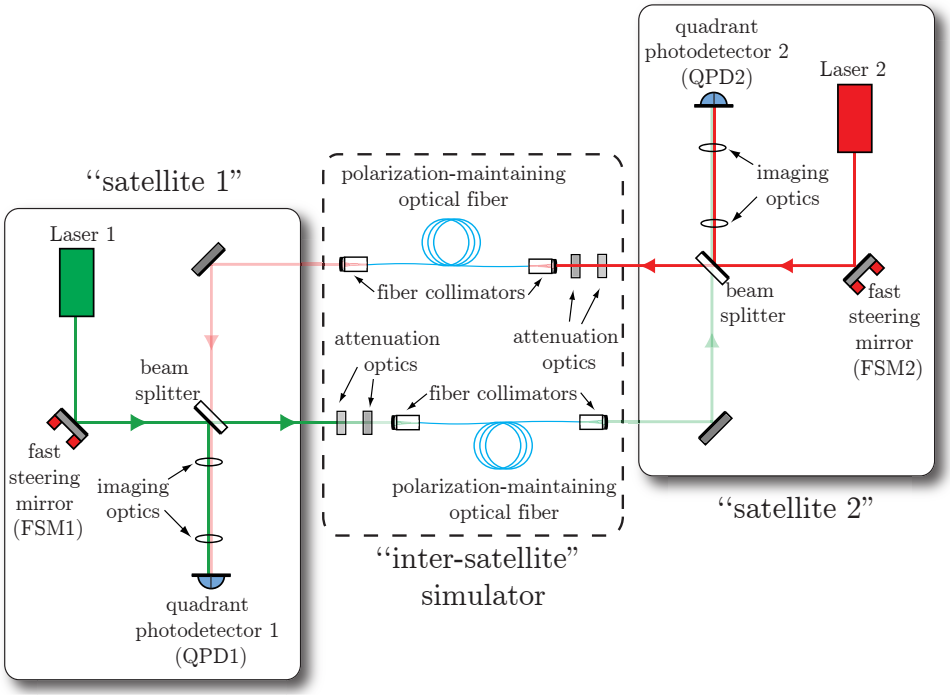

Fig. 3. Simplified experimental setup for the acquisition strategy tests showing the measurement concept and key hardware components.

instrument layout, consisting of two "satellites," each with the main hardware components listed

#208685 - $15.00 USD Received 25 Mar 2014; accepted 22 Apr 2014; published 2 May 2014

in Section 2. The lasers used were free-space NPRO lasers (Laser 1: Innolight Mephisto 200-OEM-NE-ETR, Laser 2: JDSU/Lightwave 126N-1064-700) with $\lambda = 1064$ nm. The beam waist radii planned for GFO are 2.5 mm, significantly larger than beams typically used on bench-top experiments. To achieve comparable beam sizes, we used Thorlabs F810FC-1064 collimators to produce measured beam waist radii of ~ 2 mm. Many of the optical components — such as mirrors, beam splitters, and lenses used throughout the experiment — were large 2-inch optics, and were used in the setup so as to provide plenty of range and avoid clipping when routing the large beams through the interferometer.

The steering mirrors in our experiment provide 2-axis (pitch & yaw) beam steering using voice coil actuators (Newport FSM-300 series with FSM-CD300 Controller/Driver). A photo of one of the mirrors is shown in Fig. 4. The controller reads out the mirror's position (measured internally within the FSM head) and provides fast closed-loop feedback to drive the mirror to the commanded angle, with μrad resolution and repeatability. The angular range and bandwidth of these commercial steering mirrors are similar to the flight steering mirrors [32].

The pitch θ and yaw ψ angles of the deflected beam are related to the mechanical steering mirror angles β_x and β_y by:

$$\begin{aligned} \psi &= 2\beta_x, \\ \theta &= \sqrt{2}\beta_y. \end{aligned}$$

This $\sqrt{2}$ difference between pitch and yaw is non-obvious and is present for rotations in three-dimensional geometries when reflecting off the steering mirror at 45°. These scaling factors must be applied when driving the steering mirror to deflect the beam by the desired angle.

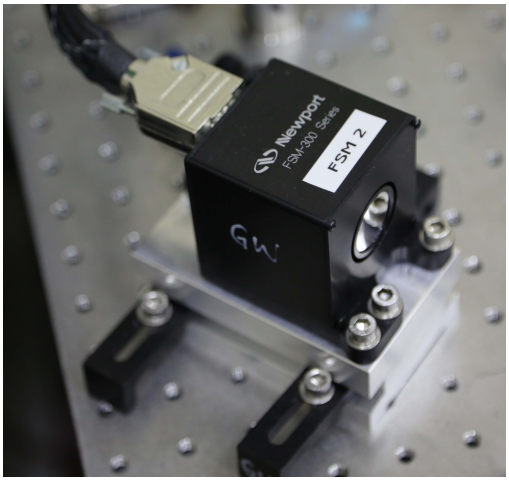

Fig. 4. Steering mirror by Newport Corporation used in experiment.

After the steering mirror, the local beam is directed to the interference beam splitter, where half of the power is directed toward the other satellite by transmitting through the beam splitter. The light reflected at the beam splitter acts as a local oscillator (LO) and interferes with the incoming light from the distant satellite, and together pass through the imaging optics. We used two lenses (f = 300 mm & f = 50 mm) to mimic the GFO telescope. Recall that the telescope images the FSM plane onto the detector. Each QPD case (housing the photodiode and detector electronics) was mounted on a 3-axis translation stage, and we fine-tuned its position in the direction along the optical axis to where the tilt-to-offset coupling was minimized through the telescope.

#208685 - $15.00 USD Received 25 Mar 2014; accepted 22 Apr 2014; published 2 May 2014

The quadrant photodetectors were built in-house, each using an InGaAs quadrant photodiode with 1 mm active area diameter (OSI FCI-InGaAs-Q1000). As the electronic noise of our high-bandwidth photodetectors (about 16 pW/$\sqrt{\text{Hz}}$ for frequencies up to 25 MHz) was slightly higher than the level anticipated for GFO [19], we increased the power in the LO beams to ensure shot noise dominated the dark noise in the photodetector output.

One challenge with experimentally testing the acquisition strategy in the laboratory was simulating the relevant characteristics of the 200 km inter-satellite separation. Note that as the local steering mirror misaligns on GFO, the beat note amplitude detected on both the local and distant satellites decreases. On the distant satellite, the beat note amplitude decreases because fewer photons reach the detector; when this beam reaches the satellite, it has a nearly-spherical wavefront and a flat-top profile over the detector area. Thus misalignments reduce the beat note amplitude predominately due to less detected power and not a reduction in contrast. The beat note amplitude decreases on the local detector, however, because of a relative tilt in wavefront between the local beam and the beam received from the other satellite, thus reducing the interferometric contrast.

To mimic this in our setup, we used attenuation optics combined with fiber collimators and polarization-maintaining optical fibers to send the beams between "satellites." This is labeled in Fig. 3 as the *inter-satellite simulator*. Misalignments of the steering mirror result in an attenuation of received power at the distant detector due to degraded coupling into the fiber. This approximately gives the correct power drop as a function of steering mirror misalignment without changing the mode shape at the distant detector.

5. Characterization

There are several important characteristics of the GFO spacecraft environment that we aimed to match in the laboratory demonstration: shot noise-limited performance, carrier-to-noise-density ratios, beat note amplitude degradation as a function of steering mirror misalignment, and representative signal processing. In this section we describe the characterization of our test bed parameters.

As mentioned previously, we increased the LO power on each detector so that shot noise dominated the photodetector electronic noise (corresponding to $\sim$ 2.5 mW LO power measured on each detector). Note that increasing the LO power does not affect the carrier-to-(shot) noise ratio. Low noise amplifiers (Mini-Circuits ZFL-500LN) were used to amplify the analog signals from each photodetector quadrant before being digitized by the ADCs. The remaining characteristics to match are discussed in further detail below.

5.1. Carrier-to-noise-density ratios

On GFO, each quadrant of the photodiode must have at least 3 pW of effective received power to ensure reliable phasemeter operation, giving a carrier-to-noise-density ratio C/N_0 of 67.5 dB-Hz per quadrant [34]. This number compares the signal power to the background white-noise power spectral density (the noise power in a 1 Hz bandwidth) [35]. Simulations predict that we can tolerate a maximum simultaneous misalignment of each steering mirror of up to $r_{wc} = 142$ μrad and still meet the minimum C/N_0 requirement per quadrant. This is determined primarily by shot noise but also includes contributions from laser intensity noise and detector electronic noise. For comparison, if both the local and signal beams were perfectly aligned, the C/N_0 would be 79.6 dB-Hz per quadrant.

To achieve representative signal power in the experiment, we set the carrier-to-noise-density ratio on any quadrant to a maximum value of 67.5 dB-Hz *or less* when both steering mirrors were misaligned by 142 μrad. This was done by adding attenuation optics and adjusting a variable neutral density filter wheel in the distant satellite's beam path (in each *inter-satellite*

#208685 - $15.00 USD Received 25 Mar 2014; accepted 22 Apr 2014; published 2 May 2014

simulator of Fig. 3) until a low enough value was reached. The exact C/N_0 value depends on the direction of the misalignment and which quadrant is viewed. For example, when both steering mirrors are misaligned by 142 μrad in yaw, the carrier-to-noise-density ratios on each quadrant ranged from 63–66.2 dB-Hz on detector 1 and 63.2–67.4 dB-Hz on detector 2. As the beat note degrades most quickly when misaligned along the 45^o axis, we set the signal power when misaligned in the x- or y-only directions to ensure that the C/N_0 would always be below 67.5 dB-Hz on any quadrant when misaligned by 142 μrad in any combination of pitch or yaw. We set the values to give us the worst-case scenario because if the peak detection algorithm can reliably find a beat note during the commissioning scan with these lower carrier-to-noise-density ratios used in our test bed, then the stronger signals expected on GFO will be comfortably found. The carrier-to-noise-density measurements were taken using a spectrum analyzer with a resolution bandwidth of 100 kHz when the lasers were phase-locked to give a beat note frequency of $\sim$ 12 MHz.

5.2. Beat note amplitude degradation with misalignment

To measure the beat note amplitude degradation as a function of misalignment, we summed the quadrants from each detector and implemented a single bin FFT algorithm on an FPGA to monitor the beat note amplitude simultaneously on each detector. We phase-locked the lasers to fix the beat note at the center of this FFT bin, $\sim$ 12 MHz, for these characterization measurements. In Fig. 5, we show the beat note amplitude of each detector when misaligning only the local beam on either satellite, normalized so that the point of highest C/N_0 has a beat note amplitude of 1. In this configuration, the distant steering mirror is kept fixed. Recall that for local beam misalignment, the beat note amplitude is degraded due to tilt between the two wavefronts. In subplots (a) and (c) the experimental data points are overlaid on the normalized beat note amplitude peak expected for GFO. Subplots (b) and (d) show contour plots of the data points for better viewing of specific pitch and yaw misalignments.

In Fig. 6, we show the beat note amplitude of each detector when misaligning only the distant beam on either satellite while keeping the local steering mirror fixed. Again we scale so at the point of highest C/N_0, the beat note amplitude equals 1. Recall that for distant beam misalignments, the beat note amplitude is reduced due to less received power.

Correspondence with the predicted GFO response is not perfect due to several effects. The dominant effect is due to the collimators producing beams with slightly smaller waist sizes, resulting in the broader peaks in Figs. 5 & 6. A second difference that affects the beat note amplitude as a function of local beam tilt is the slight difference in beam profiles. On GFO, the local beam will have a Gaussian wavefront, whereas the beam from the distant satellite will have a flat-top profile (apertured from a spherical wavefront). In our experiment, both the local and distant beams had Gaussian wavefronts, which resulted in a slightly modified beat note amplitude response.

5.3. Experiment versus GFO

The slight difference in the beat note amplitude response (between our experiment and anticipated for GFO) is allowed by the fact that we set the C/N_0 to be less than or equal to the GFO requirement within the 142 μrad misalignment cone. This means we do not run the risk of detecting signals unfairly while performing the acquisition scans. Given our slightly broader beam divergence, this means that the C/N_0 in the experiment is significantly worse than the GFO levels for better aligned cases. This nuance is not apparent from Figs. 5 and 6, where each peak has been independently scaled to equal one for zero misalignment to better illustrate the discrepancy in beam divergence.

The other complication in our laboratory demonstration that differs from GFO was the use

#208685 - $15.00 USD Received 25 Mar 2014; accepted 22 Apr 2014; published 2 May 2014

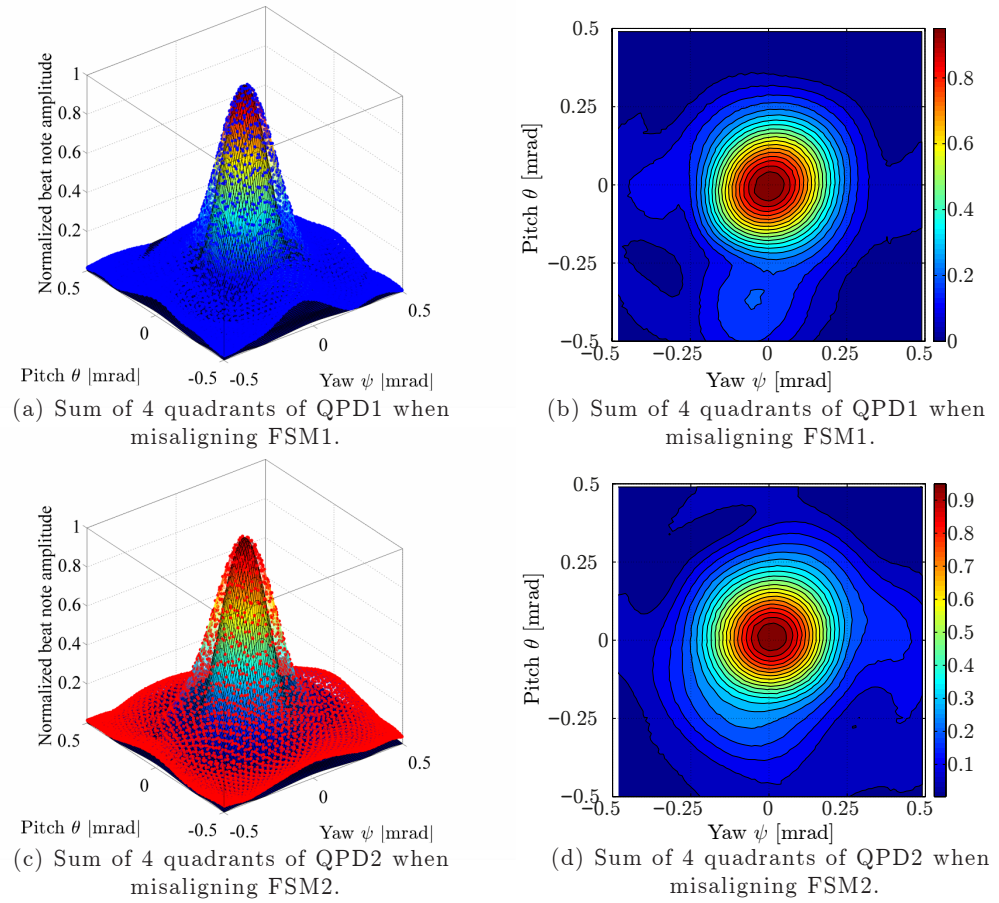

(a) Sum of 4 quadrants of QPD1 when misaligning FSM1.

(b) Sum of 4 quadrants of QPD1 when misaligning FSM1.

(c) Sum of 4 quadrants of QPD2 when misaligning FSM2.

(d) Sum of 4 quadrants of QPD2 when misaligning FSM2.

Fig. 5. Beat note amplitude versus local steering mirror misalignment with no distant beam misalignment. Subplots (a) and (c) show the experimental data points overlaid on the normalized beat note amplitude peak expected for GFO. Subplots (b) and (d) are the corresponding contour plots of the experimental data points.

of polarizing optics. As our inter-satellite simulator used fiber collimators and polarization-maintaining optical fibers, it was important to optimize the polarization state of the beams into the fibers to minimize power fluctuations due to temperature changes or mechanical stresses (e.g. in the fiber connectors). Polarcor linear polarizers (Newport 05P309AR.16) with high extinction ratios were placed before each detector so only the interference between beams in the desired polarization axis would be detected. These additions drastically improved the long-term stability of the measured beat note amplitudes.

6. Results

After carefully characterizing the experiment and matching the key parameters to make it representative of GFO, we carried out tests of the acquisition strategy. We implemented the acquisition algorithm depicted in Fig. 1 in real-time on field programmable gate arrays (National Instruments FlexRio PXIe-7966R, PXI-7852R) with a real-time controller (NI PXIe-8133). This is comparable to the signal processing hardware to be used for flight. Our ADC and primary FPGA clock were synchronized and sampled at 50 MHz (slightly higher than the 38 MHz

#208685 - $15.00 USD Received 25 Mar 2014; accepted 22 Apr 2014; published 2 May 2014

sampling frequency planned for GFO).

6.1. *Commissioning scans*

We performed many commissioning scans with the $R_{uc} = 3$ mrad uncertainty cone. Steering mirror 1 (FSM1 in Fig. 3) was driven with a Lissajous figure (x-axis frequency of 99.74 Hz, y-axis frequency of 2.77 Hz). A complete scan of FSM1 at these frequencies takes 0.36 seconds. The other steering mirror (FSM2) was driven with a hexagonal scan, starting in the center of the uncertainty cone and spiraling outwards. The steering mirror dwelled at each hexagonal scan point for 0.36 seconds (time matched to allow FSM1 to complete an entire scan), before moving to the next scan point. To cover the ± 3 mrad uncertainty cone with $r_{wc} = 142$ µrad density, 595 points are required in the hexagonal pattern. Both scan patters are shown in Fig. 2. Thus the total time to complete every combination of spatial scan points for the commissioning scan is ~ 215 seconds. On GFO, the entire sequence will be repeated as the slave laser's frequency is swept until the entire frequency uncertainty range has been covered. Depending on the rate at which the laser's frequency is swept, the spatial scan sequence could need to be repeated up

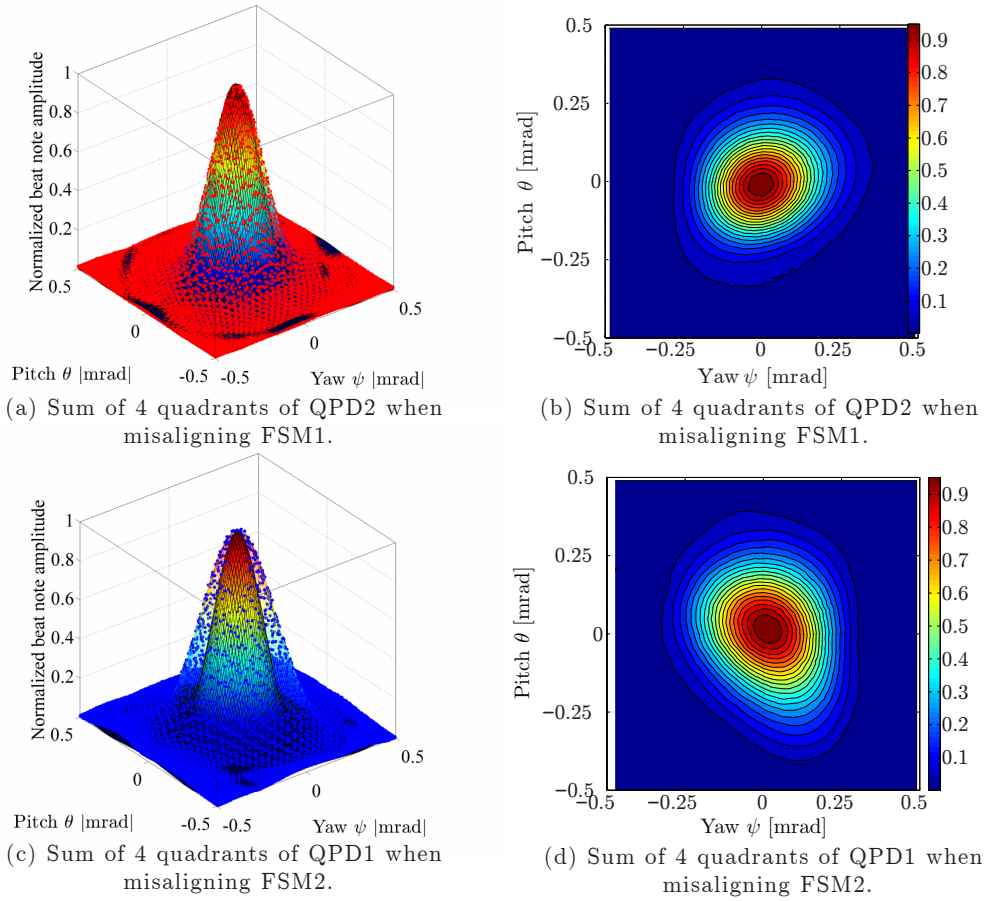

(a) Sum of 4 quadrants of QPD2 when misaligning FSM1.

(b) Sum of 4 quadrants of QPD2 when misaligning FSM1.

(c) Sum of 4 quadrants of QPD1 when misaligning FSM2.

(d) Sum of 4 quadrants of QPD1 when misaligning FSM2.

Fig. 6. Beat note amplitude versus distant steering mirror misalignment when the local beam alignment stays fixed. Subplots (a) and (c) show the experimental data points overlaid on the normalized beat note amplitude peak expected for GFO. Subplots (b) and (d) are the corresponding contour plots of the experimental data points.

#208685 - $15.00 USD Received 25 Mar 2014; accepted 22 Apr 2014; published 2 May 2014

to a few hundred times.

We vetoed all FFT frequency bins outside of 7-19 MHz. We excluded the bins above 19 MHz as this will likely be the bandwidth limit for the GFO analog chain. We excluded bins below 7 MHz to avoid false detections from excess laser relative intensity noise (RIN) at low frequencies. This RIN was larger in our experiment than expected for GRACE Follow-On due to the increased LO power needed to overcome our noisier detectors. On GFO, the value of the lower frequency bin veto will likely be around 4 MHz.

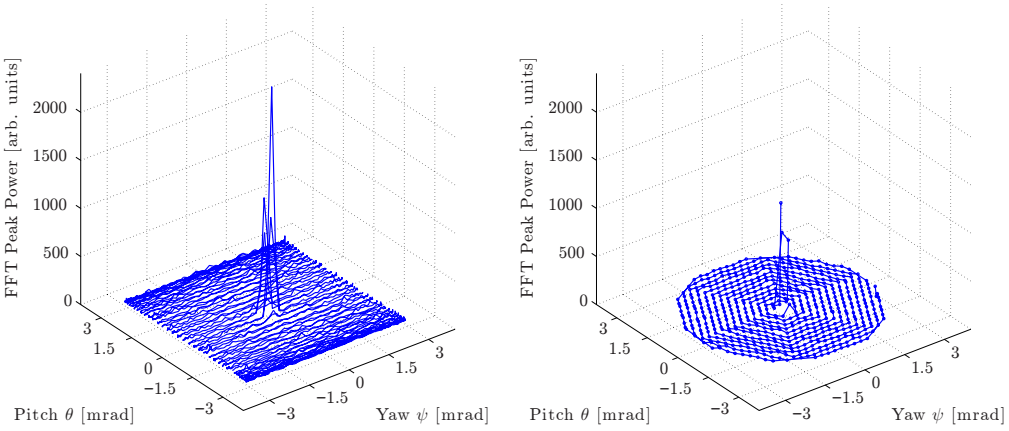

(a) Results from QPD1 versus FSM1 angle.

(b) Results from QPD2 versus FSM2 angle.

Fig. 7. Results from a worst-case scenario commissioning test where the points of highest C/N_0 are offset from the scan tracks. Both steering mirrors cover the $R_{uc} = 3$ mrad uncertainty cone with $r_{wc} = 142$ µrad resolution, with a Lissajous scan on FSM1 and a hexagonal pattern on FSM2.

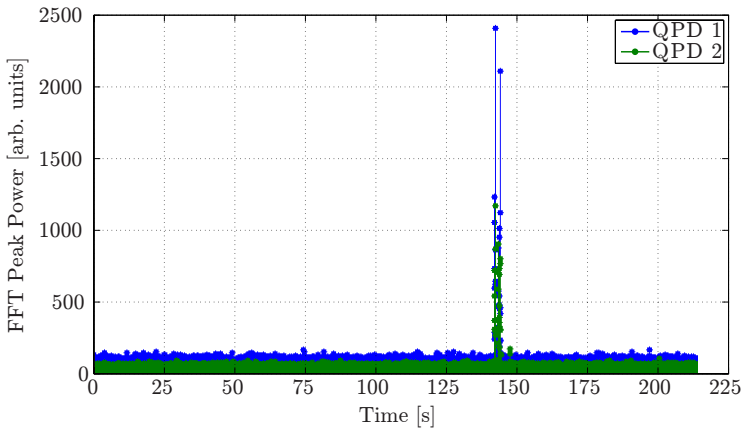

Fig. 8. A section of raw data saved during a commissioning scan showing the maximum amplitude picked for each FFT as a function of time, when the beat note frequency has come into the detection band and the alignment points are found.

In Figs. 7 & 8, we present results from one of the commissioning runs. In this measurement we intentionally selected the worst-case alignment scenario, setting angular misalignments to

#208685 - $15.00 USD Received 25 Mar 2014; accepted 22 Apr 2014; published 2 May 2014

put the point of highest C/N_0 in between the Lissajous scan tracks of FSM1 and equidistant from three adjoining scan points in the hexagonal scan pattern of FSM2. Note that for a Lissajous pattern, the largest separation of scan tracks happens near the center. For the hexagonal pattern, the scan points are uniformly separated across the entire 3 mrad uncertainty cone.

The results of Fig. 7 show the square of the maximum FFT amplitude plotted versus the steering mirror angles as the sequence sweeps through the closest alignment point. During these runs, we swept the frequency of laser 1 at 88 kHz/s (laser 2 was also free running but not swept). Even in this run where these conditions will give us the lowest C/N_0, the signal can be clearly seen in the FFT peak algorithm output of both QPD1 and QPD2, demonstrating unambiguous detection and a successful commissioning run.

The corresponding raw time domain data is shown in Fig. 8. We show a section of data covering an entire spatial scan, where the beat note frequency has been swept into the detection band and the uncertainties in all 5 degrees of freedom are found.

6.2. Reacquisition scans

As introduced previously, a fast reacquisition scan may be performed on GFO after the commissioning scan to optimize the pointing before transitioning to differential wavefront sensing. One option for the reacquisition is a quick scan with reduced angular coverage. In our reacquisition tests, the peak detection algorithm remained the same but the amplitude of each scan was reduced to ± 300 µrad. With $R_{uc} = 300$ µrad, the Lissajous pattern still takes 0.36 seconds to complete (as the driving frequencies remained unchanged), but the resolution of the scan becomes much finer ($r_{wc} = 14$ µrad). We used the same signal processing chain implemented for the commissioning scan, but scanned over only the central 19 points (of the 595 points needed for 3 mrad) in the hexagonal pattern to cover 300 µrad whilst the resolution remained at $r_{wc} = 142$ µrad. The total time to complete the reacquisition scan took 7 seconds.

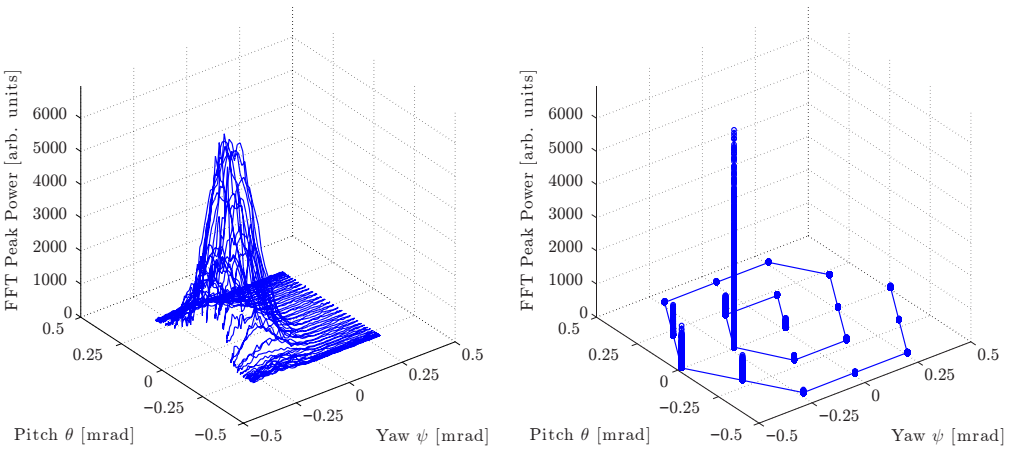

(a) Results from QPD1 versus FSM1 angle.

(b) Results from QPD2 versus FSM2 angle.

Fig. 9. Results from a reacquisition scan, with $R_{uc} = 300$ µrad. The Lissajous scan on FSM1 now has $r_{wc} = 14$ µrad resolution, while the hexagonal scan on FSM2 has $r_{wc} = 142$ µrad as before (but with fewer scan points compared to the commissioning scan).

The results of the reacquisition scan are presented in Fig. 9. Again we plot the square of the maximum FFT amplitude versus the steering mirror angles. Both lasers were free-running (this time, we did not sweep the slave laser's frequency). We vetoed the FFT frequency bins

#208685 - $15.00 USD Received 25 Mar 2014; accepted 22 Apr 2014; published 2 May 2014

as before, only keeping the bins between 7-19 MHz. Comparing Fig. 9(a) with the corresponding results from the commissioning (Fig. 7(a)), we see how the Lissajous scan with reduced amplitude maps out the interference with finer resolution. Note that the amplitude of the best alignment point in the hexagonal scan also increases, due to better alignment of the Lissajous steering mirror. FSM1 was offset by 200 μrad in the *x*-axis to highlight the significant enhancement of the finer scan, and FSM2 was offset by 300 μrad in the *x*-axis.

7. Discussion

Performing this reacquisition scan may also be necessary if the laser link is lost any time after science operation has begun. This could happen, for example, if the master laser drops lock to its reference cavity, then the laser frequency difference could jump beyond the bandwidth of the detector and wavefront sensing information would be lost. It may be possible to perform the reacquisition scan exclusively on one spacecraft, as improving the scanning resolution on just one side is enough to simultaneously enhance the beat note amplitude on both sides. This also fulfills the goal of making the reacquisition scan autonomous, with no communication between the satellites or the ground. For example, the hexagonal steering mirror could be programmed to return to the point of highest C/N_0 before the link was lost and wait. The reduced amplitude scan would be performed only on the Lissajous satellite, to find the point of highest C/N_0. The Lissajous would be steered to sit and wait at its point of highest amplitude, and after both satellites recorded several seconds of high C/N_0, differential wavefront sensing could be re-enabled.

Recall that the scanning resolution r_{wc} was initially chosen to guarantee a carrier-to-noise-density ratio strong enough to transition from the commissioning scan directly to wavefront sensing auto-alignment. By relaxing this requirement, and always requiring a reacquisition scan in between, the commissioning scan could be made sparser and therefore faster. Note a sparser scan does not necessarily mean a reduction in C/N_0 at the resulting nearest alignment point if instead of looking at the sum of the photodetector quadrants, we processed each quadrant individually. For local steering mirror misalignment, the beat note amplitude degrades more quickly for the sum of all quadrants than for an individual quadrant. This, however, would break the symmetry of the current scheme, as the beat note amplitude drop due to local or distant misalignments would no longer be near-identical. In early work we simulated a non-symmetric approach to the commissioning, but did not have time to test this approach in the laboratory.

Even if we leave the scanning resolution and signal processing unchanged, the total commissioning time could be reduced by further optimizing the spatial scan patterns. The speed at which the fast steering mirror can be moved to cover the uncertainty cone limits the speed of the total commissioning sequence, due to the finite mechanical response of the mirror. Any improvements which optimize the scanning pattern by providing more efficient coverage will directly improve (decrease) the commissioning time. An example would be to modify the Lissajous figure slightly so that the scan tracks are more evenly spaced over the uncertainty cone, increasing the frequency of the slow axis without sacrificing scan line separation.

There are several other modifications to the signal processing which could provide more robust operation or enhanced performance. We did not implement these in the experiment but discuss them as potential future improvements. One straightforward improvement is to implement a better bin vetoing algorithm. Instead of entirely rejecting all bins outside of the cutoff frequencies, a smarter bin vetoing process could enable more bins to be utilized per FFT. One possibility is a weighted approach, where an initial calibration is performed after launch to obtain the average noise in each FFT bin when no signal is present. The maximum value per FFT would be determined by finding the bin with the highest signal-to-noise ratio (instead of just the

#208685 - $15.00 USD Received 25 Mar 2014; accepted 22 Apr 2014; published 2 May 2014

highest amplitude). This increased number of usable bins per FFT could allow the slave laser's sweep rate to be increased (thus decreasing the total commissioning time).

As the beat note frequency during the scans is not constant, the amplitude measured by the FFT changes depending on the sinusoid's frequency with respect to the center of the FFT bin. The ambiguity in the amplitude (due to the random position of the beat note inside an FFT bin) could be reduced by modifying the peak detection signal processing slightly. One way to do this would be to apply a windowing function to the signal prior to the FFT. Although this makes the signal amplitude more stable, it also increases the noise due to coupling of noise from adjacent frequency bins. On average, windowing would be expected to reduce the signal-to-noise ratio and thus is not desirable when the goal is simply peak detection such as in the commissioning scan. However, in a high signal-to-noise environment, a more repeatable beat note amplitude would allow more accurate interpolation between scan lines/FFT points, which may be an advantage for the reacquisition scan.

Although feasible, it may be undesirable to use two different signal processing algorithms (un-windowed and windowed) for the commissioning and reacquisition scans. It is possible to implement something akin to windowing on the output of the FFT by taking the average of three FFT bins—the bin of maximum power as well as each bin on either side. Just as for windowing, this captures any signal power that has leaked into adjacent bins, and like windowing, incurs a noise penalty as the noise of all three bins enters the measurement. One potential penalty of this approach compared to widowing prior to the FFT is a reduced frequency resolution, but this is not a driving requirement of the acquisition strategy design. The advantage is that this alternative to windowing could be performed after the fact, either on the ground or on the flight processor, without modifying the FPGA algorithm.

8. Summary

We have experimentally demonstrated a laser link acquisition scheme in the laboratory using GRACE Follow-On parameters. We have demonstrated both the commissioning and reacquisition stages of the proposed strategy with the elected steering patterns while sweeping the frequency of the slave laser. The digital signal processing, consisting of a fast Fourier transform-based peak detection algorithm run on each photodetector output, was implemented with representative hardware. Our fast steering mirror was driven with a frequency close to the mechanical limit of the flight steering mirror. As this limit plays a large role in the total time required for the commissioning scan, our demonstration was also representative of acquisition times for GFO. In all of the commissioning and reacquisition trials performed, we unambiguously found the beat note on each detector.

The architecture for the GRACE Follow-On laser ranging instrument is now quite mature, and it is unlikely that there will be major changes to the interferometer design. The acquisition strategy continues to be refined, however, and this work augments simulations to provide risk reduction for the GRACE Follow-On laser ranging instrument.

Acknowledgments

The authors gratefully acknowledge discussions and advice from Kirk McKenzie and Andrew Sutton. This work was supported in part under the Australian Government's Australian Space Research Programme, grants from the Australian Research Council, and by the "Deutsche Forschungsgemeinschaft" (DFG) through the Cluster of Excellence QUEST (Centre for Quantum Engineering and Space-Time Research). Some of the work described in this paper was performed at the Jet Propulsion Laboratory, California Institute of Technology, under contract with the National Aeronautics and Space Administration.